Biochemical Genetics
https://doi.org/10.1007/s10528-024-10888-1

ORIGINAL ARTICLE

Familial Episodic Pain Syndrome: A Japanese Family Harboring the Novel Variant c.2431C>T (p.Leu811Phe) in *SCN11A*

Chioko Nagao[1] · Hiroko Okuda[2,7] · Gert-Jan Bekker[1] · Atsuko Noguchi[3] · Tsutomu Takahashi[3] · Akio Koizumi[2,4] · Shohab Youssefian[2,5] · Tohru Tezuka[2,5,8] · Shinji Akioka[6]

Received: 12 April 2024 / Accepted: 14 July 2024

Abstract

Familial episodic pain syndrome (FEPS) is an autosomal-dominant inherited disorder characterized by paroxysmal pain episodes. FEPS appears in early childhood, gradually disappearing with age, and pain episodes can be triggered by fatigue, bad weather, and cold temperatures. Several gain-of-function variants have been reported for *SCN9A*, *SCN10A,* or *SCN11A*, which encode the voltage-gated sodium channel α subunits Nav1.7, Nav1.8, and Nav1.9, respectively. In this study, we conducted genetic analysis in a four-generation Japanese pedigree. The proband was a 7-year-old girl, and her brother, sister, mother, and grandmother were also experiencing or had experienced pain episodes and were considered to be affected. The father was unaffected. Sequencing of *SCN9A*, *SCN10A*, and *SCN11A* in the proband revealed a novel heterozygous variant of *SCN11A*: g.38894937G>A (c.2431C>T, p.Leu811Phe). This variant was confirmed in other affected members but not in the unaffected father. The affected residue, Leu811, is located within the DII/S6 helix of Nav1.9 and is important for signal transduction from the voltage-sensing domain and pore opening. On the other hand, the c.2432T>C (p.Leu811Pro) variant is known to cause congenital insensitivity to pain (CIP). Molecular dynamics simulations showed that p.Leu811Phe increased the structural stability of Nav1.9 and prevented the necessary conformational changes, resulting in changes in the dynamics required for function. By contrast, CIP-related p.Leu811Pro destabilized Nav1.9. Thus, we speculate that p.Leu811Phe may lead to current leakage, while p.Leu811Pro can increase the current through Nav1.9.

Keywords Familial episodic pain syndrome · *SCN11A* gene · Nav1.9 · Molecular dynamics

Chioko Nagao, Hiroko Okuda and Shinji Akioka contributed equally to this work.

Extended author information available on the last page of the article

Published online: 25 July 2024

Abbreviations

ACMG	American College of Medical Genetics
CIP	Congenital insensitivity of pain
DRG	Dorsal root ganglion
FEL	Free energy landscape
FEPS	Familial episodic pain syndrome
MD	Molecular dynamics
PC	Principal component
PCA	Principal component analysis
PEM	Primary erythromelalgia
PEPD	Paroxysmal extreme pain disorder
SFN	Small fiber neuropathy
POPC	1-Palmitoyl-2-oleoyl-sn-glycero-3-phosphocholine
VGSC	Voltage-gated sodium channel
VSD	Voltage-sensing domain

Introduction

Chronic pain is a global health condition that decreases the quality of life in all generations, from newborns to the elderly. Pain sensations are generated by sensory neurons in the dorsal root ganglion (DRG), which transmit peripheral pain signals to the central nervous system. The DRG contains neurons with various receptors that transform both noxious and non-noxious stimuli into pain sensations, such as with cold exposure and low atmospheric pressure.

The voltage-gated sodium channels (VGSCs) Nav1.7, Nav1.8, and Nav1.9, encoded by *SCN9A*, *SCN10A,* and *SCN11A*, respectively, play pivotal roles in the generation of pain sensation in DRG neurons. Recent genomic analyses have revealed that VGSC variants cause the human Mendelian forms of pain-related syndromes (Bennett and Woods 2014; Shen et al. 2022). These syndromes include familial episodic pain syndrome (FEPS), small fiber neuropathy (SFN), paroxysmal extreme pain disorder (PEPD), primary erythromelalgia (PEM), and congenital insensitivity to pain (CIP) (Bennett and Woods 2014; Shen et al. 2022). FEPS, SFN, PEPD, and PEM are generally associated with gain-of-function variants in Nav1.7, Nav1.8, and Nav1.9, while CIP is related to loss-of-function variants in Nav1.7 and gain-of-function variants in Nav1.9 (Bennett and Woods 2014; Shen et al. 2022). FEPS is an autosomal-dominant inherited disorder characterized by paroxysmal pain episodes. This disorder appears in early childhood, gradually disappearing with age. Episodes are often triggered by fatigue, bad weather, or cold temperatures (Shen et al. 2022). In our previous studies, we identified several gain-of-function variants of *SCN11A* in Japanese families with FEPS (FEPS3:OMIM615552) (Kabata et al. 2018; Okuda et al. 2016).

Nav1.9, a tetrodotoxin-resistant subtype of VGSC, contributes to the generation of a persistent inward current at subthreshold voltages (Bennett et al. 2019). Interestingly, gain-of-function variants of Nav1.9 are associated with two different phenotypes, FEPS3 and CIP (HSAN7: OMIM 615548) (Bennett et al. 2019; Shen et al.

2022). By sharp contrast, Nav1.7 gain-of-function variants cause FEPS, whereas loss-of-function variants cause CIP (Bennett et al. 2019). Physiologically, gain-of-function variants of Nav1.9 are characterized by a shift in the resting membrane potential toward depolarization, making cells more excitable. Variants related to FEPS induce hyperpolarization shifts in the activation curve of less than 10 mV. By contrast, the CIP-related variant p.Leu811Pro induces a large hyperpolarization shift (more than 20 mV) in the activation voltage (Baker and Nassar 2020). Slight shifts in channel properties are considered to result in neuronal hyperexcitation, while extensive shifts are speculated to cause neuronal hypoexcitability or refractoriness (Huang et al. 2017a).

However, the intriguing nature of Nav1.9 gain-of-function variants still requires a full explanation. Gain-of-function variants related to CIP, namely c.1187T>C (p.Leu396Pro), p.Leu811Pro, and c.3904C>T (p.Leu1302Phe), are located in the transmembrane segment 6 of domain I (DI/S6), DII/S6, and DIII/S6, respectively, being in proximity to the cytosolic pore obstructing the hydrophobic gate. In silico analyses showed that PEM-associated gain-of-function variants of Nav1.7 chemically destabilized the channels, leading to a lower activation threshold relative to the wild-type or impaired steady-state fast inactivation (Huang et al. 2017b; Lampert et al. 2008).

Here, we report a four-generation pedigree with FEPS3 in which affected members have a novel variant of Nav1.9, p.Leu811Phe in DII/S6. We conducted molecular dynamics (MD) simulations of Nav1.9 to evaluate the effects of the p.Leu811Phe variant on molecular stability and conformation in the DII/S6 region, which constitutes the cytosolic pore obstructing the hydrophobic gate. Moreover, to obtain a functional insight into the potential impact of the p.Leu811Phe variant, we compared its functional effects with those of the wild-type (WT) protein and the CIP-related variant p.Leu811Pro.

Material and Methods

Human Subject and Consent Approval

The proband was from a 7-year-old girl. According to a family survey, we identified family members in which similar episodes of pain attacks had occurred since infancy. We diagnosed this family with FEPS based on pain phenotype, physical examinations, and family history. Written informed consent was obtained from all participants in compliance with the Ethics Review Board at Kyoto University (Approval No. G0501). The pedigree is shown in Fig. 1.

Genetic Analysis

Genomic DNA was extracted from the peripheral blood of the participants. All exons and intron–exon boundaries of *SCN9A*, *SCN10A*, and *SCN11A* were amplified

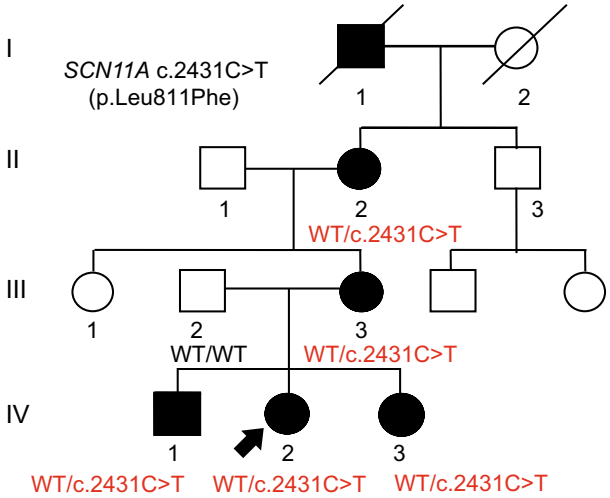

Fig. 1 Pedigree of a four-generation family with episodic pain syndrome, familial, 3 (FEPS3). Filled symbols represent affected individuals, open symbols represent unaffected individuals, squares represent males, and circles represent females. Diagonal lines indicate deceased individuals. The proband is indicated by an arrow. Genotypes of the variants are indicated at the bottom of the pedigree for each examined individual

by PCR using the indicated primer sets (Supplementary Table 1) and subjected to Sanger sequencing.

Molecular Dynamics Simulations and Structural Analysis

As no experimental structure of Nav1.9 was available within the Protein Data Bank, we obtained a predicted model from AlphaFold DB (Varadi et al. 2022) for UniProt ID Q9UI33. To simplify the simulations, the voltage-sensing domains (VSDs) and regions with low confidence scores were removed, leaving the segments Leu239–Ala416, Pro685–Leu823, Thr1148–Ser1341, and Arg1481–Ser1614. We created three systems from this model: the WT plus two variants, p.Leu811Phe and p.Leu811Pro. Each system was embedded in a hexagonal membrane consisting of 70% 1-Palmitoyl-2-oleoyl-sn-glycero-3-phosphocholine (POPC) and 30% cholesterol (Bekker et al. 2021a). Subsequently, water was added, along with 0.1 M of NaCl and additional ions to neutralize each system. MD simulations were performed using the Amber99SB-ILDN force field (Lindorff-Larsen et al. 2010), lipid14 (Dickson et al. 2014), monovalent ion parameters (Joung and Cheatham 2008), and TIP3P (Jorgensen et al. 1983) to parameterize the protein segments, membrane molecules, ions, and water molecules, respectively. Energy minimizations, followed by 100 ps NVT and NPT simulations with position restraints on the heavy solute atoms, were used to prepare the system, with the final WT system shown in Fig. 4. Gromacs 2022.3 [https://doi.org/10.5281/zenodo.7037338] was used to prepare and perform the simulations. For each system, a production run was executed lasting 1 μs per

trajectory, with three trajectories per system, initialized with a short, restrained 100 ps NVT simulation and random velocities. The production run simulations were performed with the NPT ensemble, and snapshots were saved at 10 ps intervals, giving 300,000 structures per system.

We performed principal component analysis (PCA) and K-means clustering as described previously (Bekker et al. 2020, 2021a, b; Bekker and Kamiya 2021, 2022). The array consisted of intramolecular Cα atoms between i (Leu396-Cα, Ile807-Cα, Ile1304-Cα, Ile1600-Cα, Tyr375-Cα, Tyr1198-Cα) and all Cα atoms j in the structure, excluding the highly flexible extracellular loop region (Leu281–Asp343, Gly724–Trp755, Gly1202–Asn1242, Ser1269–Asn1281, Asn151–Thr1536, Ser1558–Ile1579), as well as excluding Cα atoms of residues j within $i \pm 3$. The structures were projected onto the first two principal components (PCs), yielding a 2D histogram from which the probability of each bin (P_i) could be calculated. Using P_i, the free energy as the potential of mean force was calculated, and 2D free energy landscapes (FELs) were obtained.

After the PCA, we performed K-means clustering on the data, using $k' = 100$ clusters and a set of PC dimensions such that the sum of the contributions to the variance exceeded 90%, corresponding to PC1–PC20. For each cluster, one representative structure was then selected, and the clusters were ranked based on the number of structures assigned to each cluster, k' (i.e., the probability of each cluster). Using these representative structures, we performed a direct analysis of structural similarity using R-value analysis (Bekker et al. 2019a, b). The R-value quantifies the degree to which intra- and/or inter-molecular contacts are preserved with respect to a reference structure. Starting from the most stable cluster, $k' = 1$, in order of the size of each cluster, representative structures with an R-value > 0.925 were merged. This gave us k number of clusters and the corresponding representative structures $\mathbf{r}_k$, for each system.

We determined the pore radius using the HOLE program (Smart et al. 1996). Using the data from the final 400 ns of each trajectory, snapshots at 10 ns intervals (0.1% of the trajectory data) were superposed using all Cα atoms and analyzed using the HOLE program. For additional details, see supplementary information.

Results

Clinical Phenotype

A 7-year-old girl (IV-2 in Fig. 1) born to nonconsanguineous parents was referred to our clinic because she had been experiencing persistent pain in both hands and feet since the age of two.

The pain was paroxysmal, happening suddenly, unrelated to exercise, and lasting 20–30 min before abruptly disappearing. The attacks would happen any time of day, being more common during the evening but not uncommon during the morning. When a pain attack occurred, the girl was immobilized and had to crouch down. She experienced pain localized to the wrist and leg (from the thigh to the ankle joint), occurring in multiple areas simultaneously, or within a single site. Oral non-steroidal

anti-inflammatory drugs were ineffective for the pain, but acetaminophen enabled her to move unassisted within 30 min of ingesting medication. She did not experience coldness, burning sensations, numbness, paresthesia, or motor paralysis at the site of pain. The attacks occurred approximately twice a week and the frequency was only slightly influenced by external factors such as weather, season, and outside temperature. No other type of pain (such as headache or abdominal pain) was noted. Physical examination did not reveal any other abnormalities throughout the body. According to a family survey, while the father (III-2) of the proband was unaffected, her siblings (IV-1 and IV-3), mother (III-3), maternal grandmother (II-2), and great-grandfather (I-1) all experienced similar pain attack episodes since infancy. Within the family, attack frequency gradually diminished with age, and the mother, grandmother, and great-grandfather had experienced only a few attacks in adulthood. Based on the characteristic episodes of pain attacks and family history, the family was suspected to be suffering from FEPS, an inherited pain disorder.

Genetic Analysis via Sanger Sequencing

Sequencing of *SCN9A*, *SCN10A*, and *SCN11A* in the proband (IV-2) revealed a heterozygous variant of *SCN11A*: NC_000003.12:g.38894937G>A, (NM_001349253.2:c.2431C>T, NP_001336182.1:p.Leu811Phe) (Fig. 2).

This novel single nucleotide variant was not present in the gnomAD population database (https://gnomad.broadinstitute.org/), Exome Variant Server (https://evs.gs.washington.edu/EVS/), dbSNP (https://www.ncbi.nlm.nih.gov/snp/), 1000 Genomes

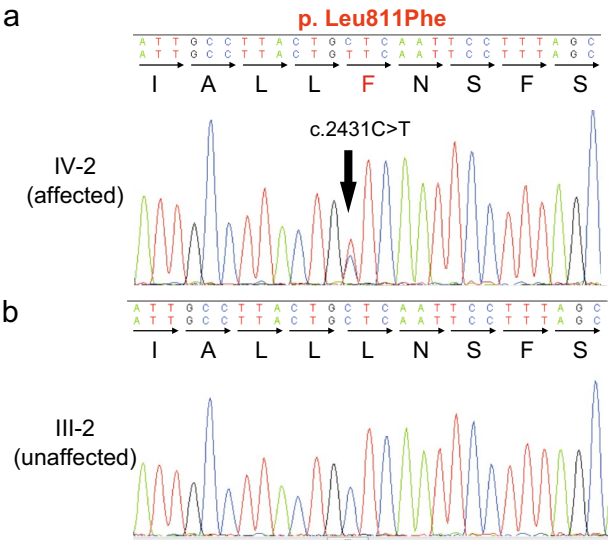

Fig. 2 Sanger sequencing chromatograph. **a** Sequence from the affected proband (IV-2) showing the heterozygous *SCN11A* variant g.38894937G>A (c.2431C>T, p.Leu811Phe). **b** Sequence from the unaffected father (III-2), without the Leu811 variant

Project (https://www.internationalgenome.org/), or ClinVar disease database (https://www.ncbi.nlm.nih.gov/clinvar/). No other coding variants or structural changes such as deletions or copy number variations were found in any of the sequenced regions in *SCN9A*, *SCN10A*, or *SCN11A*. This variant was also identified in IV-1, 3, III-3, and II-2, who had experienced similar pain attack episodes, but not in III-2, who did not exhibit the pain phenotype. I-1 was not available for genomic analysis. Alignment of the Nav1.9 amino acid sequence with other sodium channels and Nav1.9 proteins from other species indicated that the Leu811 residue was highly conserved (Fig. 3). The pathogenicity prediction programs PolyPhen-2 (Adzhubei et al. 2010) and SIFT (Ng and Henikoff 2003) predicted this p.Leu811Phe change to be probably damaging (score: 1) and deleterious (score: 0.01), respectively. The CADD score for this variant is 25.4 (Schubach et al. 2024). In addition, this variant was classified as "pathogenic" (PS4, PM1, PM2, PM5, PP1, PP3 and PP4) according to the American College of Medical Genetics (ACMG) guidelines (Richards et al. 2015). Therefore, this variant is likely to be pathogenic.

Molecular Dynamics Simulations

To evaluate the structural effects of the *SCN11A* variants, we prepared model systems of the pore regions of the WT protein (Fig. 4), p.Leu811Phe variant, and CIP-related p.Leu811Pro variant, and performed MD simulations. The FELs of the structural ensembles projected onto the first two PCs are shown in Fig. 5. The WT and p.Leu811Phe FELs both consisted of two connected basins, which were more closely connected in the p.Leu811Phe FEL, whereas the p.Leu811Pro system consisted of three unconnected basins. These results suggested the p.Leu811Phe variant to be more stable than the WT, as all parallel trajectories sampled the same region in the PC1/PC2 space. By contrast, the three unconnected basins in the p.Leu811Pro system, where each basin corresponded to a different parallel trajectory, suggested that p.Leu811Pro was less stable than the WT protein. This was especially notable in the initial conformation at the start of the simulations, as each trajectory quickly diverged, finally ending up at these different semi-stable conformations. As inspection of representative structures around the variant site can also provide some detail regarding the motion captured by each PC, we selected three structures each for the WT and p.Leu811Phe systems and five for the p.Leu811Pro system for further analysis (Fig. 5). Comparing the structures WT_$\mathbf{r}_3$ and p.Leu811Phe_$\mathbf{r}_2$ (Fig. 6a), which had similar PC2 values but differed considerably in their PC1 values, suggested that the DIII/S6 helix had moved upwards (i.e., away from the intracellular side) in p.Leu811Phe. Moreover, as the conformation of the terminal of the DII/S6 section (S815) also differed between the structures, the fold of this section also seemed to correlate with PC1. Comparing WT_$\mathbf{r}_1$/p.Leu811Phe_$\mathbf{r}_2$ and p.Leu811Pro_$\mathbf{r}_1$ (Fig. 6b), which differed greatly along PC2 and somewhat along PC1, showed a deformation near Leu811, along with several other changes.

We also analyzed the effects of the variants on pore radius along the pore of the molecule (ensemble averages and standard deviations are plotted in Fig. 7a, b, respectively), with each system showing different characteristics. Leu811 was located at around

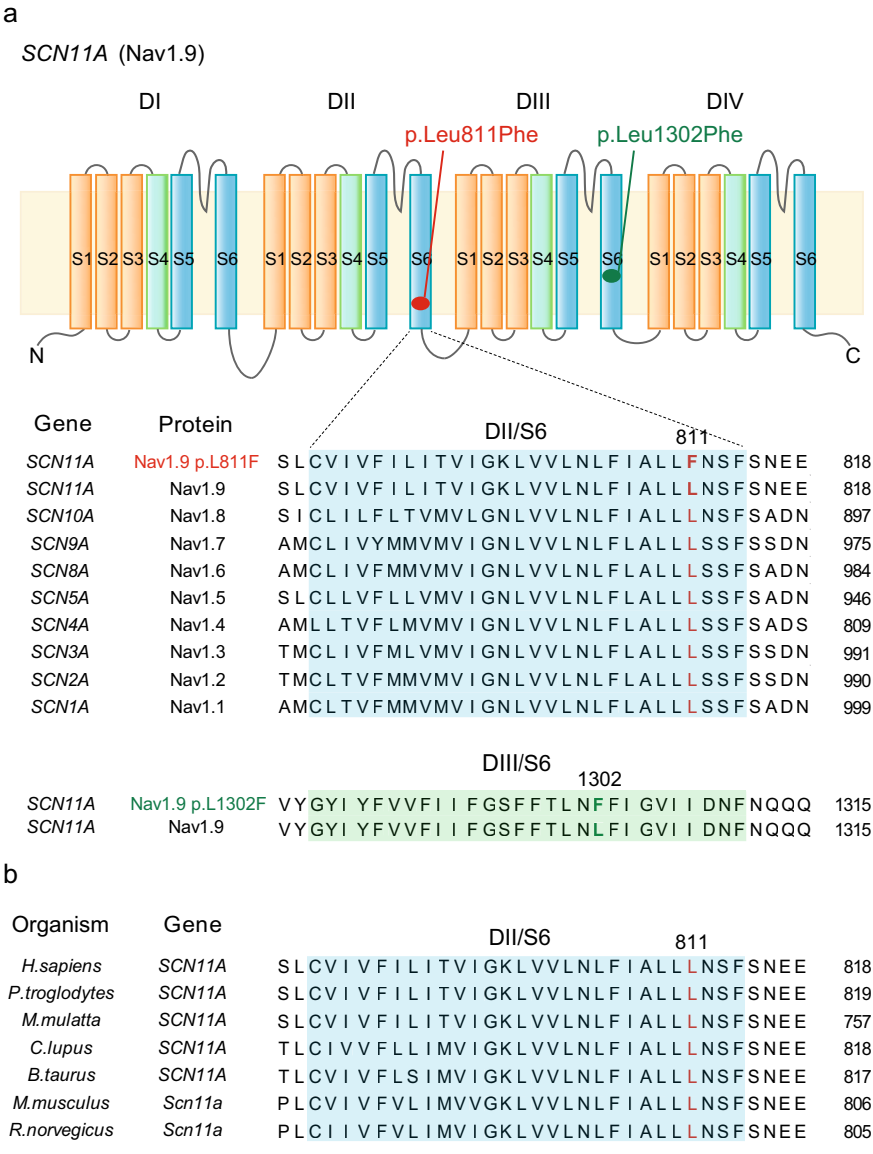

Fig. 3 Schematic diagram of Nav1.9 and locations of variants in pain and painless disorders. **a** The Nav channel consists of four domains (DI–DIV), with each domain consisting of six transmembrane segments (S1–S6). The novel painful p.Leu811Phe variant and painless p.Leu1302Phe variant are indicated by the red and green dots, respectively. The lower panels show the alignment of the S6 transmembrane segments of DII (light blue background) of human Nav1.1–1.9 and DIII (light green) of human Nav1.9. Leu811 in DII (red) and Leu1302 in DIII (green) of Nav1.9 are highly conserved hydrophobic amino acid residues in DII/S6 and DIII/S6, respectively. The reference sequences are as follows: Nav1.9, NP_001336182.1; Nav1.8, NP_006505.4; Nav1.7, NP_001352465.1; Nav1.6, NP_001317189.1; Nav1.5, NP_000326.2; Nav1.4, NP_000325.4; Nav1.3, NP_008853.3; Nav1.2, NP_001035232.1; and Nav1.1, NP_001159435.1. **b** Multiple sequence alignment of the DII/S6 conserved regions of seven Nav1.9 orthologs using CLUSTALW2. The leucine residue (L; red) is highly conserved in each ortholog. The reference sequences are as follows: *H.sapiens*, NP_054858.2; *P.troglodytes*, XP_003309747.1; *M.mulatta*, XP_001083888.1; *C.lupus*, XP_542712.5; *B.taurus*, XP_002696965.1; *M.musculus*, NP_036017.3; *R.norvegicus*, NP_062138.1. (color figure online)

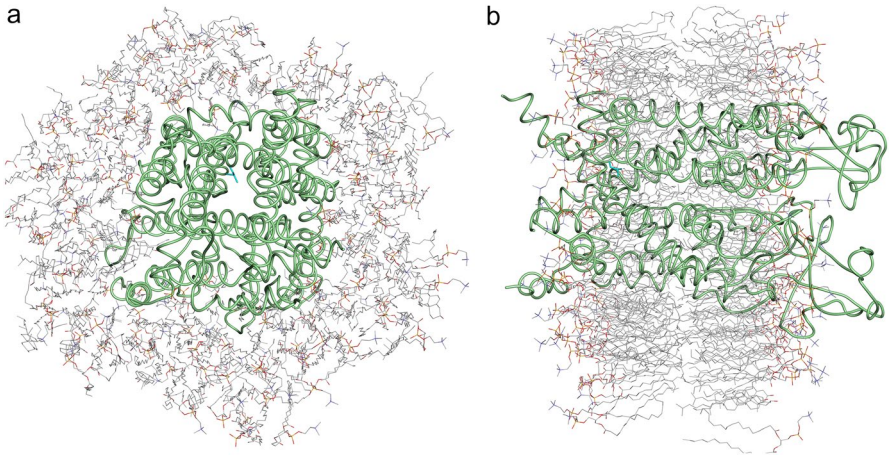

Fig. 4 Overview of the prepared WT system. **a** The WT system viewed from the intracellular side with Leu811 shown as a stick model (light blue). **b** Side view of the system along the pore. Nav1.9 segments are shown as green tubes, and the POPC and cholesterol molecules are shown as stick models with CPK coloring. The images were produced using Molmil (Bekker et al. 2016), a WebGL based molecular viewer developed by PDBj (Bekker et al. 2022; Kinjo et al. 2017). (color figure online)

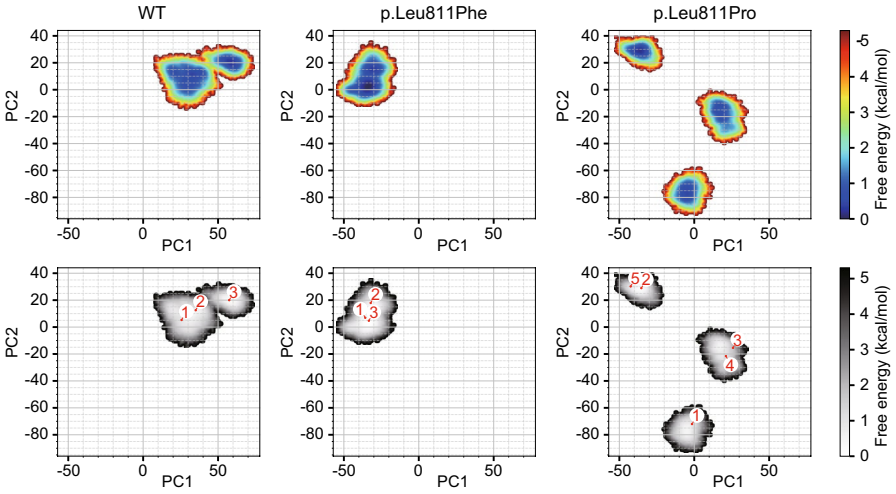

Fig. 5 Free energy landscapes in WT Nav1.9 and variants. The panels on the top show the free energy landscape (FEL) of each system (WT, p.Leu811Phe, and p.Leu811Pro); the panels on the bottom show the FELs, along with the location on the FELs of representative structures selected from each ensemble. The FELs have been normalized so that the densest region of all three systems corresponds to 0 kcal/mol

36 Å, which corresponds to the location of the pore gate in the WT, and the minimum observed radius was also located here. On the other hand, for the p.Leu811Pro system, the minimum radius was slightly closer to the intracellular region, at around 34 Å. For p.Leu811Phe, the minimum radius was located in between that of the WT and

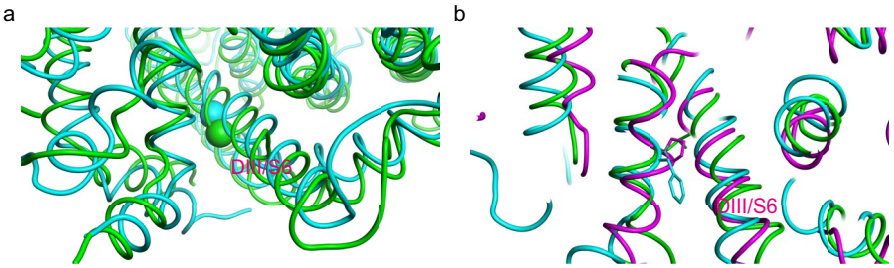

Fig. 6 Conformational changes observed among representative structures selected from the system ensembles. **a** Comparison between WT_$\mathbf{r}_3$ (green) and p.Leu811Phe_$\mathbf{r}_2$, (cyan), with the Cα atom of Leu1302 indicated as a sphere and the location of DIII/S6 indicated. **b** Comparison between WT_$\mathbf{r}_1$ (green), p.Leu811Phe_$\mathbf{r}_2$ (cyan), and p.Leu811Pro_$\mathbf{r}_1$ (magenta), with the sidechain of Leu811/Phe811/Pro811 shown as a stick model and DIII/S6 indicated. (color figure online)

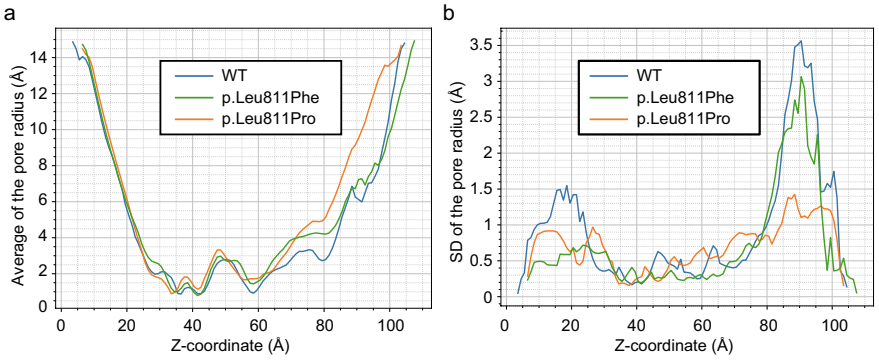

Fig. 7 Comparison of pore radius along the channel in WT, p.Leu811Phe, and p.Leu811Pro. **a** Average pore radius measured over the MD ensemble of the WT (blue), p.Leu811Phe (green), and p.Leu811Pro (orange) systems along the channel. **b** Standard deviation of the pore radius measured over the MD ensemble of the WT, p.Leu811Phe, and p.Leu811Pro systems along the channel. (color figure online)

p.Leu811Pro systems and was not as narrow. Furthermore, looking at the fluctuation of the pore radius suggested that the WT was quite flexible around the pore gate, while p.Leu811Pro was the most stable and p.Leu811Phe was in between them in terms of the stability of the pore gate. Notably, p.Leu811Phe showed higher fluctuation of the pore radius next to the pore gate (at around 38 Å), but overall tended to be more stable along the whole pore (30–80 Å). This suggests that the p.Leu811Phe variant induces a somewhat higher fluctuation to its nearby region, while stabilizing the pore region as a whole.

Discussion

We previously identified six *SCN11A* variants in 17 unrelated Japanese families with FEPS (Kabata et al. 2018; Okuda et al. 2016). In this study, we examined an additional patient with similar pain episodes and found a novel variant in *SCN11A*, designated g.38894937G>A (c.2431C>T, p.Leu811Phe), in a four-generation Japanese family with FEPS. The clinical characteristics of this pedigree were similar to those of previously reported pedigrees (Kabata et al. 2018; Leipold et al. 2015; Okuda et al. 2016; Zhang et al. 2013): onset in early childhood, attenuation in adulthood, no redness, or swelling at painful sites, no symptoms in the intermittent period, and no complications of motor disorders or mental retardation. The painful sites were commonly located in the distal extremities, but the exact locations varied between family members or changed with age in the same patient. In the present case, the pain radiated from the knee joint to surrounding areas, similar to another case with a c.3551T>C (p.Val1184Ala) variant (Kabata et al. 2018). These findings indicate that the site of pain is not simply determined by the variant, and patients with FEPS3 do not show uniform expression of pain. Pain attacks are triggered by cold temperatures and bad weather in most patients with FEPS3, such as those carrying c.665G>A (p.Arg222His), c.673C>T (p.Arg225Cys), c.3437T>C (p.Phe1146Ser) and p.Val1184Ala variants. However, in the present family, attacks were not triggered by weather conditions, as observed in patients carrying the c.2441T>G (p.Phe814Cys) variant (Kabata et al. 2018). As both Leu811 and Phe814 are located in the DII/S6 region of Nav 1.9, the location of the variant may be related to triggers of pain attacks. Meanwhile, autonomic symptoms like intractable constipation and drug efficacy have been reported in various ways (Shen et al. 2022), even within the same pedigree. Besides the variant type of *SCN11A*, predisposing factors such as age of onset or duration of illness may affect the clinical picture of FEPS3.

This p.Leu811Phe variant is of particular interest because mutation of amino acid 811 from leucine to proline (p.Leu811Pro) is reported to induce CIP (Leipold et al. 2013), suggesting that the variant we report here may cause topological changes that are sensitive to signal transduction. Although we did not experimentally prove p.Leu811Phe to be a gain-of-function variant, we consider this mutation likely to be pathogenic for the following reasons. First, this variant is absent from the population database. Second, this variant completely segregated subjects with and without pain episodes for three generations in this family. Third, Polyphen-2, SIFT, CADD, and ACMG classifications all predicted p.Leu811Phe as a pathologic variant. Finally, the MD simulations suggested that this variant changes the stability and conformational preference of Nav1.9, which could alter its signal transduction properties.

The FELs obtained from the MD simulation trajectories showed that incorporating the p.Leu811Phe variant resulted in stabilization of the conformation of Nav1.9. By contrast, the p.Leu811Pro variant caused destabilization of the Nav1.9 structure, which fluctuated between several conformations corresponding to local minima. Structural stabilization observed with the p.Leu811Phe variant throughout the pore may prevent the necessary conformational changes in the pore domain. Feasibly, this could result in a shortened response cycle and

persistent failure of the channel to fully open/close. Therefore, we speculate that p.Leu811Phe may induce current leakage from Nav1.9, as the structure has difficulty operating in distinct open and closed states and instead appears to prefer a more intermediary state. Conversely, in the case of the p.Leu811Pro variant, the local rigidness of the proline induced structural instability of the pore domain, especially around the middle of the pore near the VSD and could, therefore, increase the time taken to open and close the pore, leading to an increase in Nav1.9 current.

Taken together, our results suggest that mutation of Leu811 may not only affect protein stability and the local conformation, but may also influence the dynamics required for the normal sodium channel functioning, thereby leading to the observed gain-of-function in FEPS or the loss-of-function observed in CIP.

The mechanism by which each Nav 1.9 mutation causes FEPS or CIP also requires further study. For example, p.Arg222His, the most frequent variant in FEPS3 (Kabata et al. 2018), potentially causes gain-of-function by a different mechanism than p.Leu811Phe, as reported by Han et al. (2017). They used a modeling analysis to show that p.Arg222His, located in the VSD (not included in our computational analysis), decreases stability of the resting state by hindering the formation of salt bridges in the VSD. They suggested this would enable an easier transition to an open state, resulting in a shift of voltage-dependent channel activation towards hyperpolarization, as indicated by a change in the half-maximum activation voltage and an increase in window current (Han et al. 2017). Therefore, the mechanisms through which p.Leu811Phe and p.Arg222His induce pain might be different: p.Leu811Phe results in structural stabilization, while p.Arg222His might lead to destabilization.

Nav1.9 is considered to primarily affect the resting membrane potential. A hyperpolarization shift of activation of less than 10 mV has been observed in FEPS, whereas hyperpolarization shifts in activation/deactivation of more than 20 mV have been observed as a result of the CIP-related p.Leu811Pro and p.Leu1302Phe variants (Baker and Nassar 2020). Several studies have suggested that the resting membrane potential is one of the factors that determines the threshold for cell activation (Baker and Nassar 2020; Bennett et al. 2019), and that depolarizing changes that are too large inhibit action potential generation, causing a decrease in excitability (Huang et al. 2017a). The proximity of Leu1302 and Leu811 to the VSD suggests that changes in dynamics, coupled with a change of signal transduction from the VSD, may lead to a significant increase in sodium ion influx and potentially cause CIP. Therefore, proper conformational stability and dynamics are essential for correct signaling of Nav1.9.

In the present study, we had a major limitation. We did not use a physiological method (such as voltage clamp or current clamp) to directly demonstrate that *SCN11A* p.Leu811Phe causes hyperexcitation. In a future study, further physiological examination, including the use of behavioral and electrophysiological analyses of a relevant knock-in mouse model, combined with structural determination by X-ray crystallography/cryo-electron microscopy and large-scale MD simulations, is warranted to elucidate the pathogenicity of the p.Leu811Phe variant and the mechanism(s) by which p.Leu811Pro causes CIP and p.Leu811Phe causes FEPS.

Conclusions

We demonstrated a novel missense variant, *SCN11A* p.Leu811Phe, in a four-generation family with FEPS. The rarity, segregation, and pathogenicity prediction programs suggested this variant to be likely pathogenic. MD analysis demonstrated that the p.Leu811Phe variant affected both protein stability and conformation, increasing the molecular rigidity along the pore region of the channel. By contrast, a CIP counterpart variant, p.Leu811Pro, decreased structural stability. As such, *SCN11A* p.Leu811Phe may induce current leakage as a result of slower conformational change, resulting in a physiological gain-of-function phenotype.

Supplementary Information The online version contains supplementary material available at https://doi.org/10.1007/s10528-024-10888-1.

Acknowledgements This work was supported by the Collaborative Research Program of Institute for Protein Research, Osaka University (CRa-23-04). We would like to thank the HPCI Research Project (hp220002) for providing us with the computational resources of the TSUBAME3.0 system, Tokyo Institute of Technology. We also thank Sarah Ivins, PhD, and Rachel James, PhD, from Edanz (https://jp.edanz.com/ac), and Ethan Sahker, PhD (Graduate School of Medicine, Kyoto University) for editing a draft of this manuscript.

Authors' Contributions CN and GJB performed three-dimensional analysis and drafted the manuscript; HO and TTe participated in genetic analysis and drafted the manuscript. AN and TTa critically revised the manuscript for important intellectual content; AK and YS drafted and critically revised the manuscript for important intellectual content, and supervised the study; SA participated in the patient's follow-up and data-gathering and drafted the manuscript. All authors have read and approved the manuscript.

Funding This work was funded by AlphaNavi Pharma Inc. and supported by MHLW Research on the Rare and Intractable diseases Program (Grant Number: JPMH19FC1003 and JPMH22FC1006) and the Grand-in-Aid for Scientific Research from the Japan Society for the Promotion of Science (Grant Number: JP20H03229).

Availability of Data and Materials The datasets generated and/or analyzed during the current study are deposited in the NCBI dbSNP repository, [https://www.ncbi.nlm.nih.gov/SNP/snp_ss.cgi?ss=2137544419]. The representative structures and interactive versions of Figs. 4 and 6 have been submitted to the Biological Structure Model Archive (BSM-Arc), under BSM-00052 (https://doi.org/10.51093/bsm-00052, on hold until publication).

Declarations

Conflict of interest The authors declare the following conflict of interests: HO, AK, and TTe report personal fees from AlphaNavi Pharma during the study period. AN, TTa, and AK have a patent pending regarding *SCN11A* (name of patent, 'Pain gene and its applications'; Japanese Patent Application No. P2016-098215A). Rest all authors have no conflicting interest to disclose.

Ethical Approval The study design was approved by the Ethics Review Board of Kyoto University (Approval No. G0501, Approval date Aug. 2nd, 2012).

Consent to Participate Written informed consent for participation in this study was obtained from all participants. For children, written informed consent was obtained from their parents.

Consent for Publication Written informed consent for the publication of genetic and clinical data was obtained from all participants. The parents of the children signed written informed consent for the publication of genetic and clinical data.

References

Adzhubei IA, Schmidt S, Peshkin L, Ramensky VE, Gerasimova A, Bork P, Kondrashov AS, Sunyaev SR (2010) A method and server for predicting damaging missense mutations. Nat Methods 7(4):248–249. https://doi.org/10.1038/nmeth0410-248

Baker MD, Nassar MA (2020) Painful and painless mutations of *SCN9A* and *SCN11A* voltage-gated sodium channels. Pflugers Arch 472(7):865–880. https://doi.org/10.1007/s00424-020-02419-9

Bekker GJ, Kamiya N (2021) N-Terminal-driven binding mechanism of an antigen peptide to human leukocyte antigen-A*2402 elucidated by multicanonical molecular dynamic-based dynamic docking and path sampling simulations. J Phys Chem B 125(49):13376–13384. https://doi.org/10.1021/acs.jpcb.1c07230

Bekker GJ, Kamiya N (2022) Advancing the field of computational drug design using multicanonical molecular dynamics-based dynamic docking. Biophys Rev 14(6):1349–1358. https://doi.org/10.1007/s12551-022-01010-z

Bekker GJ, Nakamura H, Kinjo AR (2016) Molmil: a molecular viewer for the PDB and beyond. J Cheminform 8(1):42. https://doi.org/10.1186/s13321-016-0155-1

Bekker GJ, Araki M, Oshima K, Okuno Y, Kamiya N (2019a) Dynamic docking of a medium-sized molecule to its receptor by multicanonical MD simulations. J Phys Chem B 123(11):2479–2490. https://doi.org/10.1021/acs.jpcb.8b12419

Bekker GJ, Ma B, Kamiya N (2019b) Thermal stability of single-domain antibodies estimated by molecular dynamics simulations. Protein Sci 28(2):429–438. https://doi.org/10.1002/pro.3546

Bekker GJ, Araki M, Oshima K, Okuno Y, Kamiya N (2020) Exhaustive search of the configurational space of heat-shock protein 90 with its inhibitor by multicanonical molecular dynamics based dynamic docking. J Comput Chem 41(17):1606–1615. https://doi.org/10.1002/jcc.26203

Bekker GJ, Araki M, Oshima K, Okuno Y, Kamiya N (2021a) Accurate binding configuration prediction of a G-protein-coupled receptor to its antagonist using multicanonical molecular dynamics-based dynamic docking. J Chem Inf Model 61(10):5161–5171. https://doi.org/10.1021/acs.jcim.1c00712

Bekker GJ, Fukuda I, Higo J, Fukunishi Y, Kamiya N (2021b) Cryptic-site binding mechanism of medium-sized Bcl-xL inhibiting compounds elucidated by McMD-based dynamic docking simulations. Sci Rep 11(1):5046. https://doi.org/10.1038/s41598-021-84488-z

Bekker GJ, Yokochi M, Suzuki H, Ikegawa Y, Iwata T, Kudou T, Yura K, Fujiwara T, Kawabata T, Kurisu G (2022) Protein data bank Japan: celebrating our 20th anniversary during a global pandemic as the Asian hub of three dimensional macromolecular structural data. Protein Sci 31(1):173–186. https://doi.org/10.1002/pro.4211

Bennett DL, Woods CG (2014) Painful and painless channelopathies. Lancet Neurol 13(6):587–599. https://doi.org/10.1016/S1474-4422(14)70024-9

Bennett DL, Clark AJ, Huang J, Waxman SG, Dib-Hajj SD (2019) The role of voltage-gated sodium channels in pain signaling. Physiol Rev 99(2):1079–1151. https://doi.org/10.1152/physrev.00052.2017

Dickson CJ, Madej BD, Skjevik AA, Betz RM, Teigen K, Gould IR, Walker RC (2014) Lipid14: the amber lipid force field. J Chem Theory Comput 10(2):865–879. https://doi.org/10.1021/ct4010307

Han C, Yang Y, Te Morsche RH, Drenth JP, Politei JM, Waxman SG, Dib-Hajj SD (2017) Familial gain-of-function Na(v)1.9 mutation in a painful channelopathy. J Neurol Neurosurg Psychiatry 88(3):233–240. https://doi.org/10.1136/jnnp-2016-313804

Huang J, Vanoye CG, Cutts A, Goldberg YP, Dib-Hajj SD, Cohen CJ, Waxman SG, George AL Jr (2017a) Sodium channel NaV1.9 mutations associated with insensitivity to pain dampen neuronal excitability. J Clin Invest 127(7):2805–2814. https://doi.org/10.1172/JCI92373

Huang W, Liu M, Yan SF, Yan N (2017b) Structure-based assessment of disease-related mutations in human voltage-gated sodium channels. Protein Cell 8(6):401–438. https://doi.org/10.1007/s13238-017-0372-z

Jorgensen WL, Chandrasekhar J, Madura JD, Impey RW, Klein ML (1983) Comparison of simple potential functions for simulating liquid water. J Chem Phys 79(2):926–935. https://doi.org/10.1063/1.445869

Joung IS, Cheatham TE 3rd (2008) Determination of alkali and halide monovalent ion parameters for use in explicitly solvated biomolecular simulations. J Phys Chem B 112(30):9020–9041. https://doi.org/10.1021/jp8001614

Kabata R, Okuda H, Noguchi A, Kondo D, Fujiwara M, Hata K, Kato Y, Ishikawa K, Tanaka M, Sekine Y et al (2018) Familial episodic limb pain in kindreds with novel Nav1.9 mutations. PLoS ONE 13(12):e0208516. https://doi.org/10.1371/journal.pone.0208516

Kinjo AR, Bekker GJ, Suzuki H, Tsuchiya Y, Kawabata T, Ikegawa Y, Nakamura H (2017) Protein Data Bank Japan (PDBj): updated user interfaces, resource description framework, analysis tools for large structures. Nucleic Acids Res 45(D1):D282–D288. https://doi.org/10.1093/nar/gkw962

Lampert A, O'Reilly AO, Dib-Hajj SD, Tyrrell L, Wallace BA, Waxman SG (2008) A pore-blocking hydrophobic motif at the cytoplasmic aperture of the closed-state Nav1.7 channel is disrupted by the erythromelalgia-associated F1449V mutation. J Biol Chem 283(35):24118–24127. https://doi.org/10.1074/jbc.M802900200

Leipold E, Liebmann L, Korenke GC, Heinrich T, Giesselmann S, Baets J, Ebbinghaus M, Goral RO, Stodberg T, Hennings JC et al (2013) A *de novo* gain-of-function mutation in *SCN11A* causes loss of pain perception. Nat Genet 45(11):1399–1404. https://doi.org/10.1038/ng.2767

Leipold E, Hanson-Kahn A, Frick M, Gong P, Bernstein JA, Voigt M, Katona I, Oliver Goral R, Altmuller J, Nurnberg P et al (2015) Cold-aggravated pain in humans caused by a hyperactive NaV1.9 channel mutant. Nat Commun. https://doi.org/10.1038/ncomms10049

Lindorff-Larsen K, Piana S, Palmo K, Maragakis P, Klepeis JL, Dror RO, Shaw DE (2010) Improved side-chain torsion potentials for the Amber ff99SB protein force field. Proteins 78(8):1950–1958. https://doi.org/10.1002/prot.22711

Ng PC, Henikoff S (2003) SIFT: Predicting amino acid changes that affect protein function. Nucleic Acids Res 31(13):3812–3814. https://doi.org/10.1093/nar/gkg509

Okuda H, Noguchi A, Kobayashi H, Kondo D, Harada KH, Youssefian S, Shioi H, Kabata R, Domon Y, Kubota K et al (2016) Infantile pain episodes associated with novel Nav1.9 mutations in familial episodic pain syndrome in Japanese families. PLoS ONE 11(5):e0154827. https://doi.org/10.1371/journal.pone.0154827

Richards S, Aziz N, Bale S, Bick D, Das S, Gastier-Foster J, Grody WW, Hegde M, Lyon E, Spector E et al (2015) Standards and guidelines for the interpretation of sequence variants: a joint consensus recommendation of the American College of Medical Genetics and Genomics and the Association for Molecular Pathology. Genet Med 17(5):405–424. https://doi.org/10.1038/gim.2015.30

Schubach M, Maass T, Nazaretyan L, Roner S, Kircher M (2024) CADD v1.7: using protein language models, regulatory CNNs and other nucleotide-level scores to improve genome-wide variant predictions. Nucleic Acids Res 52(D1):D1143–D1154. https://doi.org/10.1093/nar/gkad989

Shen Y, Zheng Y, Hong D (2022) Familial episodic pain syndromes. J Pain Res 15:2505–2515. https://doi.org/10.2147/JPR.S375299

Smart OS, Neduvelil JG, Wang X, Wallace BA, Sansom MS (1996) HOLE: a program for the analysis of the pore dimensions of ion channel structural models. J Mol Graph 14(6):354–360, 376. https://doi.org/10.1016/s0263-7855(97)00009-x

Varadi M, Anyango S, Deshpande M, Nair S, Natassia C, Yordanova G, Yuan D, Stroe O, Wood G, Laydon A et al (2022) AlphaFold protein structure database: massively expanding the structural coverage of protein-sequence space with high-accuracy models. Nucleic Acids Res 50(D1):D439–D444. https://doi.org/10.1093/nar/gkab1061

Zhang XY, Wen J, Yang W, Wang C, Gao L, Zheng LH, Wang T, Ran K, Li Y, Li X et al (2013) Gain-of-function mutations in *SCN11A* cause familial episodic pain. Am J Hum Genet 93(5):957–966. https://doi.org/10.1016/j.ajhg.2013.09.016

Authors and Affiliations

Chioko Nagao[1] · Hiroko Okuda[2,7] · Gert-Jan Bekker[1] · Atsuko Noguchi[3] · Tsutomu Takahashi[3] · Akio Koizumi[2,4] · Shohab Youssefian[2,5] · Tohru Tezuka[2,5,8] · Shinji Akioka[6]

✉ Tohru Tezuka
tezuka.toru.8w@kyoto-u.ac.jp

✉ Shinji Akioka
sakioka@koto.kpu-m.ac.jp

[1] Institute for Protein Research, Osaka University, Osaka, Japan

[2] Department of Pain Pharmacogenetics, Graduate School of Medicine, Kyoto University, Kyoto, Japan

[3] Department of Pediatrics, Akita University School of Medicine, Akita, Japan

[4] Institute of Public Health and Welfare, Kyoto-Hokenkai, Kyoto, Japan

[5] Laboratory of Molecular Biosciences, Graduate School of Medicine, Kyoto University, Kyoto, Japan

[6] Department of Pediatrics, Graduate School of Medical Science, Kyoto Prefectural University of Medicine, Kyoto, Japan

[7] Present Address: Department of Preventive Medicine, St. Marianna University School of Medicine, Kanagawa, Japan

[8] Present Address: Laboratory of Integrative Molecular Medicine, Graduate School of Medicine, Kyoto University, Kyoto, Japan